AMERICAN SOCIETY FOR MICROBIOLOGY | mBio®

RESEARCH ARTICLE

Kinetic Tracking of *Plasmodium falciparum* Antigens on Infected Erythrocytes with a Novel Reporter of Protein Insertion and Surface Exposure

Jinfeng Shao,[a] Gunjan Arora,[b] Javier Manzella-Lapeira,[b] Joseph A. Brzostowski,[b] Sanjay A. Desai[a]

[a]Laboratory of Malaria and Vector Research, National Institute of Allergy and Infectious Diseases, National Institutes of Health, Rockville, Maryland, USA
[b]Laboratory of Immunogenetics, National Institute of Allergy and Infectious Diseases, National Institutes of Health, Rockville, Maryland, USA

ABSTRACT Intracellular malaria parasites export many proteins into their host cell, inserting several into the erythrocyte plasma membrane to enable interactions with their external environment. While static techniques have identified some surface-exposed proteins, other candidates have eluded definitive localization and membrane topology determination. Moreover, both export kinetics and the mechanisms of membrane insertion remain largely unexplored. We introduce Reporter of Insertion and Surface Exposure (RISE), a method for continuous nondestructive tracking of antigen exposure on infected cells. RISE utilizes a small 11-amino acid (aa) HiBit fragment of NanoLuc inserted into a target protein and detects surface exposure through high-affinity complementation to produce luminescence. We tracked the export and surface exposure of CLAG3, a parasite protein linked to nutrient uptake, throughout the *Plasmodium falciparum* cycle in human erythrocytes. Our approach revealed key determinants of trafficking and surface exposure. Removal of a C-terminal transmembrane domain aborted export. Unexpectedly, certain increases in the exposed reporter size improved the luminescence signal, but other changes abolished the surface signal, revealing that both size and charge of the extracellular epitope influence membrane insertion. Marked cell-to-cell variation with larger inserts containing multiple HiBit epitopes suggests complex regulation of CLAG3 insertion at the host membrane. Quantitative, continuous tracking of CLAG3 surface exposure thus reveals multiple factors that determine this protein's trafficking and insertion at the host erythrocyte membrane. The RISE assay will enable study of surface antigens from divergent intracellular pathogens.

IMPORTANCE Malaria parasites invade and replicate within red blood cells of their human or animal hosts to avoid immune detection. At the same time, these parasites insert their own proteins into the host membrane to scavenge plasma nutrients, facilitate immune evasion, and perform other essential activities. As there is broad interest in developing vaccines and antimalarial therapies against these surface-exposed antigens, robust methods are needed to examine how and when parasite proteins insert at the host membrane. We therefore developed and used Reporter of Insertion and Surface Exposure (RISE) to track parasite antigen exposure. Using RISE, we followed the time course of membrane insertion for CLAG3, a conserved protein linked to a nutrient uptake channel on infected erythrocytes. We found that CLAG3 insertion occurs at specific parasite stages and that this insertion is required for the formation of the nutrient uptake channel. We also varied the size and charge of the extracellular domain to define constraints on protein insertion at the host membrane. Single-cell imaging revealed that some cells continued to export CLAG3 even with large extracellular loops, suggesting sophisticated strategies used by malaria parasites to control their interactions with host plasma.

KEYWORDS NanoLuc, ion channels, malaria, membrane insertion, nutrient uptake, protein export, protein trafficking

Editor L. David Sibley, Washington University School of Medicine

Address correspondence to Sanjay A. Desai, sdesai@niaid.nih.gov.

The authors declare no conflict of interest.

Received 15 February 2022
Accepted 18 March 2022
Published 14 April 2022

Many viral, bacterial, and parasitic microbes invade, grow, and replicate within human and animal cells to evade immune detection, access host cell machinery for replication, and use cellular macromolecules as nutrient sources (1). At the same time, the intracellular milieu limits the pathogen from accessing plasma nutrients and often provides an inhospitable ionic composition or acidic pH. To overcome these hurdles, intracellular pathogens often export effector proteins into their host cell to remodel their abode, altering host cell defenses and physiology to their benefit (2–4). A subset of effector proteins then insert in the host membrane to enable pathogen interactions with the extracellular space. These exposed proteins serve diverse roles and are acknowledged vaccine and drug targets.

In the virulent human malaria parasite *Plasmodium falciparum*, surface-exposed proteins benefit pathogen replication by facilitating cytoadherence (5), immune evasion (6), and nutrient uptake (7). These antigens have been identified through static assays, such as confocal and electron microscopy techniques. Because these methods lack the required spatial resolution (8), they cannot unambiguously determine if some parasite proteins are surface exposed or only adherent to the inner membrane face or cytoskeleton. Susceptibility to extracellular proteases or antibody-based assays with live cells can resolve this uncertainty (9–11), but these approaches also have limitations. Another approach, namely, mass spectrometry-based identification after surface labeling with *N*-hydroxysuccinimide (NHS) esters (12), has yielded a largely unvalidated list of proteins that is complicated by increased NHS ester permeability after infection with *Plasmodium* spp. (13).

To better understand host membrane insertion and functional properties of parasite antigens, new methods to track these surface-exposed proteins are needed. Notably, both surface exposure via fusion of exocytic vesicles and "punch-through" insertion of soluble protein into the host membrane have been proposed (14, 15), but the absence of direct and quantitative measurements has prevented definitive mechanistic insights.

To address these limitations and better define how pathogen proteins insert at their host cell membrane, we developed and used Reporter of Insertion and Surface Exposure (RISE). Our study combines RISE with biochemical studies of CLAG3, a critical determinant of parasite nutrient acquisition, to examine trafficking and membrane insertion of this surface-exposed antigen.

RESULTS

HiBiT tagging within a conserved surface antigen in malaria parasites. We sought to generate a sensitive kinetic reporter for protein insertion on infected cells and chose human erythrocytes infected with the virulent *P. falciparum* malaria parasite. Indirect immunofluorescence microscopy assays (IFAs) with antibodies against exposed epitopes offer a specific readout but suffer from low spatial resolution and provide limited kinetic information about protein export and host membrane insertion. Split enzyme reporters can overcome these limitations when one enzyme fragment is introduced into the exported protein; a specific signal is produced through complementation with a second fragment added extracellularly. Similar location-specific complementation has been described using mammalian proteins (16), but this approach has not been used to track the appearance of pathogen-derived antigens on host cells. Because it relies on extracellular interactions with a surface-exposed epitope, our strategy resembles antigen presentation on immune effector cells (17).

The bright NanoLuc luciferase is an ideal enzymatic reporter for blood-stage *P. falciparum* studies (18) and has recently been optimized for the development of a split reporter (19). We selected the 11 residue HiBiT and 18-kDa LgBiT fragments of NanoLuc for our studies, based on their strong association (equilibrium dissociation constant [K_D] = 700 pM) that yields an ATP-independent, furimazine-sensitive luminescence signal.

We next reasoned that minimal modification of a normally exported parasite protein would be more informative about parasite biology than extensively engineered reporters, as used previously (20). We preferred the parasite CLAG3 protein for these studies over antigens such as PfEMP1 and RIFINs encoded by large multigene families to avoid epigenetic regulation and variable expression (21). *Clag* paralogs also undergo

epigenetic silencing (22), but some clones carry a single constitutively expressed hybrid *clag3* gene termed *clag3h* (23). One such line, KC5, has been used successfully for transfections without the risk of epigenetic silencing (24). CLAG3 is also the only known surface-exposed protein conserved in all examined *Plasmodium* spp. (25), suggesting that trafficking insights made using this protein may be broadly applicable. Because CLAG3 expression is linked to the plasmodial surface anion channel (PSAC), an ion and nutrient uptake channel at the host membrane (10), transport studies with transfectant parasites would also provide a biochemical correlate of reporter signal activity. We therefore selected CLAG3 for tagging and the KC5 clone for the production of a surface exposure reporter parasite.

CLAG3 has a small 10- to 30-amino acid (aa) hypervariable region that appears to be exposed at the host membrane (hypervariable region [HVR], Fig. 1A) (26). We therefore used CRISPR-Cas9 editing to replace the KC5 *clag3h* HVR sequence with a single HiBiT tag flanked by 8-aa linker sequences; we named this limiting dilution clone *8-1* based on the size of the flanking linker and the number of inserted HiBiT tags (Fig. 1A, bottom). HVR replacement increased the size of the extracellular loop domain by a modest 10 residues (see Fig. S1A in the supplemental material). We also produced *8-1HA*, a similar line with a hemagglutinin (HA) epitope tag added after the HiBiT linker cassette. Two additional lines, namely, *8-1trunc* and *8-1HAtrunc*, express truncated CLAG3 reporters with a stop codon introduced after the inserted cassette (Fig. 1A, bottom, and Fig. S1A in the supplemental material). We initially reasoned that these truncation constructs would yield a more flexible extracellular HiBiT epitope and provide insights into roles served by the downstream CLAG3 sequence. Although CLAG3 is a critical determinant of PSAC activity, CLAG3 knockout parasites are viable (27), possibly because other CLAG paralogs in *P. falciparum* compensate for CLAG3 loss. Thus, we expected that our modifications would not be lethal to transfected parasites unless they produce a dominant negative effect on nutrient uptake (28).

Immunoblotting with each cloned transfectant confirmed expression and revealed single bands of expected size. Probing with anti-CLAG3 confirmed the loss of this antibody's C-terminal epitope in the *8-1trunc* clone and unchanged electrophoretic migration in *8-1* (Fig. 1B, top). Both engineered CLAG3 isoforms were identified using a LgBiT probe that binds to HiBiT-tagged proteins to produce a luminescence signal (Fig. 1B, bottom); the KC5 parent was not recognized by LgBiT, confirming the specificity of this probe for the HiBiT tag. Similar results were obtained in the HA tandem-tagged parasites (Fig. 1C), establishing faithful expression.

IFAs confirmed and extended these findings. At the schizont stage, we detected each variant shortly after stage-specific synthesis under the genomic *clag3h* promoter (Fig. 1D, top group of images). While *8-1 HA* parasites trafficked the modified CLAG3 protein normally to developing rhoptries, the truncated tagged protein in *8-1HAtrunc* produced a more diffuse pattern with a small fraction reaching the rhoptry to colocalize with RhopH3, an associated protein that also contributes to PSAC formation (29).

At merozoite egress and reinvasion, rhoptry proteins are secreted into the next erythrocyte and deposited into the parasitophorous vacuole (30). From there, through a presumed but poorly understood interaction with the PTEX translocon, CLAG3 is exported into the host cytosol for trafficking to the host membrane (29, 31). Imaging revealed that the tandem-tagged CLAG3 protein in *8-1HA* trafficked as expected and colocalized with RhopH3 at the host cell surface (Fig. 1D, bottom group); an antibody specific for the CLAG3 C terminus further confirmed this localization (see Fig. S1B in the supplemental material). In contrast, the truncated CLAG3 in *8-1HAtrunc* parasites was less abundant, suggesting that its poor trafficking to rhoptries compromised delivery to the next erythrocyte upon reinvasion. The small pool of this protein delivered into trophozoites failed to be exported and did not colocalize with RhopH3 (Fig. 1D, bottom row).

We next used luminescence blotting to detect the stage-specific abundance of HiBit-tagged proteins. This approach resembles traditional immunoblots and is based on the visualization of HiBiT-tagged proteins via the luminescence generated upon

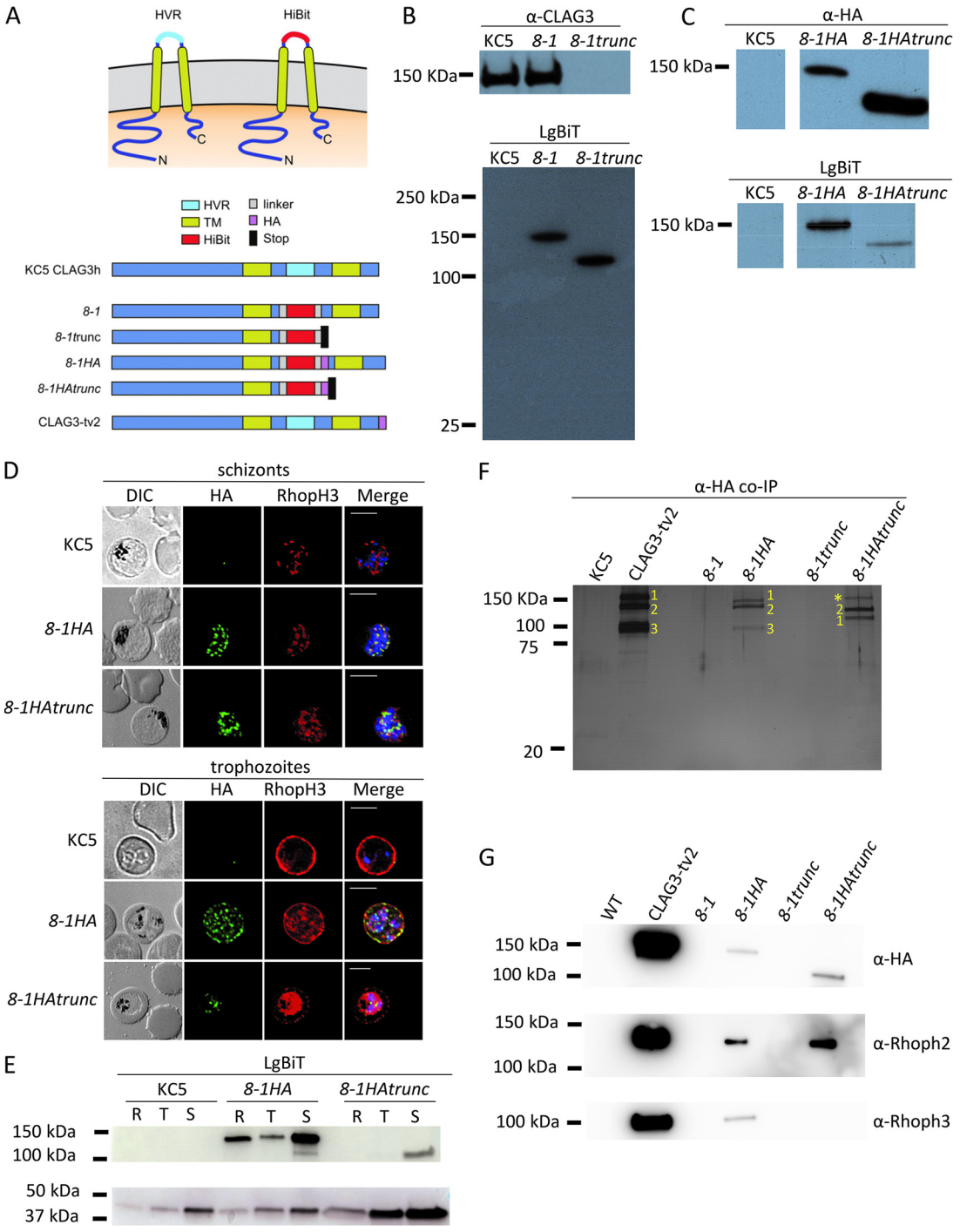

FIG 1 Design and production of host membrane-exposed split-reporter antigens. (A) Schematic shows native and modified CLAG3 topology at the host erythrocyte surface (left and right top images, respectively). The native HVR sequence is replaced by varied HiBiT reporter cassettes. Engineered lines are shown with ribbon diagrams at the bottom. (B) Immunoblots of matched total cell lysates from indicated lines, probed with antibody against a C-terminal CLAG3 epitope (top) or with LgBiT (bottom). *8-1trunc* is recognized by LgBiT but not by anti-CLAG3. (C) Immunoblots showing recognition of HA-tagged lines with anti-HA and LgBiT. (D) Indirect immunofluorescence assays (IFAs) of indicated proteins in wild-type (WT) and transfected lines. In schizonts (top), CLAG3 colocalizes with RhopH3 in apical rhoptries (puncta) in *8-1HA* but has a more diffuse distribution in *8-1HAtrunc*. IFA with trophozoite-stage parasites (bottom) reveals a normal export of CLAG3 and colocalization with RhopH3 at the host membrane in *8-1HA* but a reduced signal with failed export in *8-1HAtrunc*. Scale bars, 5 mm. (E) Immunoblots showing stage-specific CLAG3 abundance in indicated lines (top row, probed with LgBiT). The truncated protein in *8-1HAtrunc* is detected in schizonts (S) but not rings or trophozoites (R and T). Bottom row, aldolase loading control. (F) Silver-stained gel showing coimmunoprecipitation using anti-HA beads and indicated parasite lysates. WT, *8-1*, and *8-1trunc* represent no-HA negative controls. Yellow 1, 2, and 3 labels indicate CLAG3, RhopH2, and RhopH3, respectively. The asterisk label may reflect recovery of CLAG paralogs from other chromosomes, consistent with previous studies that suggest CLAG hetero-oligomerization to form PSAC (27). (G) Immunoblots using eluates from F, probed with indicated antibodies; anti-HA recognizes the CLAG3 bait protein (n = 1 for α-RhopH2, ≥3 for other antibodies).

LgBiT complementation. When performed with *8-1HA* parasites, it revealed increases in CLAG3 abundance upon parasite maturation to the schizont stage (Fig. 1E), consistent with the synthesis of this and other RhopH proteins predominantly in the late-stage parasites (32). Ring and trophozoite parasites contained smaller amounts that reflect an incomplete transfer from prior cycle schizonts during egress and reinvasion (29). The truncated protein in *8-1HAtrunc* was detected in schizonts but not in ring- and trophozoite-stage parasites, further implicating a role of the CLAG3 C-terminal region in efficient transfer to rhoptries and new erythrocytes during invasion. This observation is consistent with prior studies showing rapid degradation of CLAG3 in schizonts when stabilizing interactions with RhopH2 and RhopH3 are disrupted (29).

We next used coimmunoprecipitation on anti-HA beads to examine protein-protein interactions for these CLAG3 reporter proteins (Fig. 1F, silver-stained gel). CLAG3 was recovered from *8-1HA* and *8-1HAtrunc* lysates but not from negative-control *8-1* and *8-1trunc* lines (bands labeled "1", Fig. 1F), confirming specific pulldown. RhopH2 and RhopH3, unrelated proteins that interact with CLAG3 (25), were recovered from *8-1HA* (bands labeled "2" and "3," Fig. 1F), albeit with lower efficiency than in experiments using CLAG3-tv2, an engineered control parasite that expresses a full-length CLAG3 with a C-terminal HA epitope tag (Fig. 1A) (31). This reduced yield may result from compromised binding and recovery with an internal HA epitope tag compared with the C-terminal tag in CLAG3-tv2. Coimmunoprecipitation using *8-1HAtrunc* yielded an unchanged RhopH2 band and a smaller band as expected for truncated CLAG3, but RhopH3 was not detected in these silver-stained gels (Fig. 1F). Immunoblotting confirmed recovery of RhopH2 with each modified parasite; RhopH3 was successfully recovered in pulldowns using *8-1HA* but not in those using *8-1HAtrunc* (Fig. 1G). The recent cryo-electron microscopy (cryo-EM) RhopH complex structure reveals that CLAG3 interacts with RhopH3 via two primary domains termed the CLAG3 "300 region" and "1300 loop" (31, 33). Because the 1300 loop is distal to the site of CLAG3 truncation in *8-1HAtrunc*, these findings suggest that this loop is required for a stable CLAG3-RhopH3 interaction.

Kinetics of membrane insertion and surface exposure. We next monitored stage-specific CLAG3 surface exposure on infected erythrocytes with the RISE method. We measured luminescence resulting from complementation of the HiBiT tag by extracellular LgBiT (Fig. 2A). Bioluminescence microscopy revealed an undetectable reporter signal on immature ring-infected erythrocytes (Fig. 2B, left panels) on KC5 and both HiBiT tagged lines, consistent with the appearance of PSAC activity on infected cells only after parasite maturation (34). In contrast, trophozoite-infected cells exhibited a surface-distributed luciferase signal specific to *8-1* (Fig. 2B and C). The *8-1trunc* parasite matured normally but failed to produce a surface signal.

We then miniaturized this reporter assay into 96-well microplate wells and tracked CLAG3 exposure kinetics in cultures initiated shortly after invasion. Although both clones exhibited negligible signals for the first 16 h of the parasite cycle, this lag was followed by a rapid increase in CLAG3 membrane insertion to produce luminescence on *8-1* (Fig. 2D, red circles). This signal reached a plateau between 30 and 44 h on *8-1*, during which *8-1trunc* parasites continued to produce minimal luminescence. At the end of the erythrocyte cycle (44 to 48 h), both transfectant cultures exhibited abruptly increased signals, consistent with merozoite egress and CLAG3 discharge into extracellular medium (32). At the signal plateau, approximately one-third of the CLAG3 within *8-1* infected cells had become surface exposed based on the measured reporter signal before and after detergent release (Fig. 2E, 36-h time point).

We used transfection to produce two negative-control parasites (see Fig. S2 in the supplemental material). *GBP-HB* expresses 5 tandem HiBit tags behind a leader sequence from GBP130, a soluble parasite protein exported into host cytosol (35). *C3-cHB* is a CLAG3 diploid line that expresses a full-length CLAG3 protein with a C-terminal tandem HiBit tag; this tag is expected to remain intracellular based on CLAG3 topology

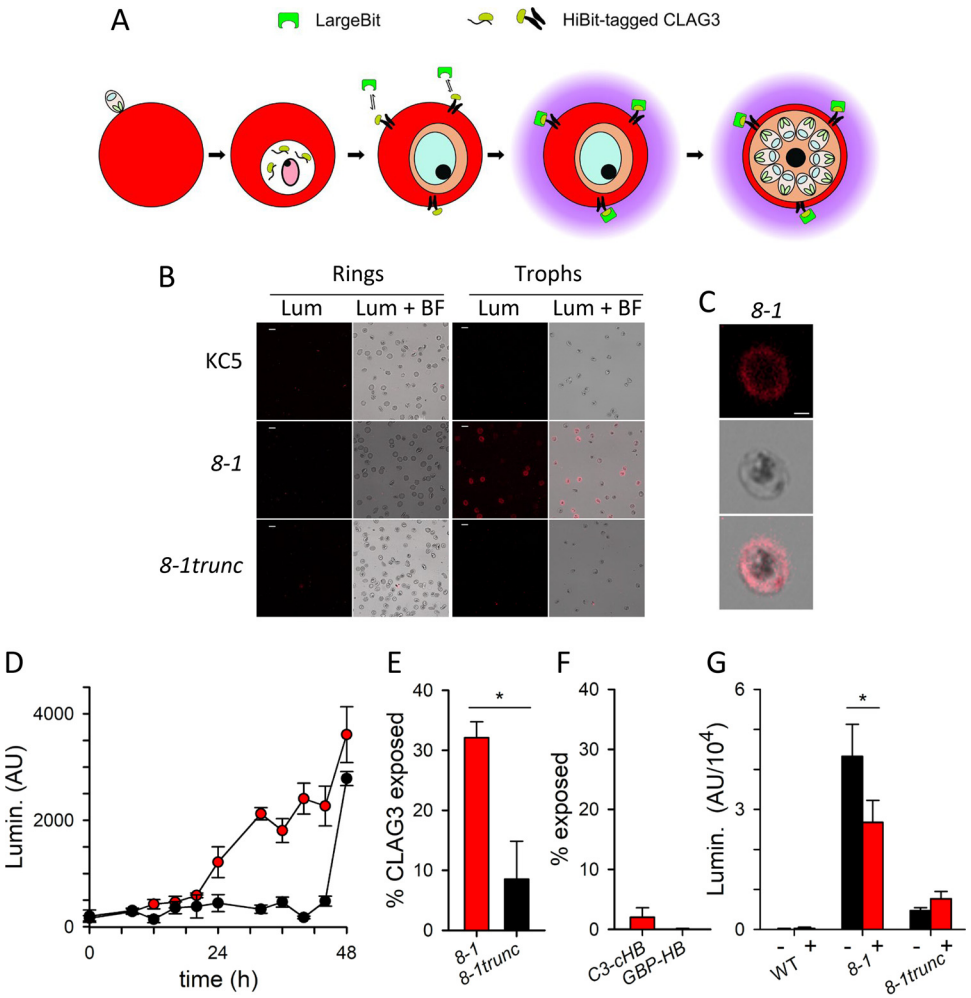

FIG 2 Faithful tracking of host membrane insertion. (A) Schematic showing parasite developmental stages and host membrane insertion-dependent luminescence. After invasion, the tagged CLAG3 protein is deposited into the parasitophorous vacuole before export and eventual insertion at the host membrane. Interaction between extracellular LgBiT and the surface-exposed HiBiT tag on *8-1* yields luminescence at mature parasite stages (purple glow). (B) Bioluminescence microscopy images showing undetectable signals on immature ring-infected cells (left) but a bright luminescence signal on *8-1* infected cells at the trophozoite stage (right). KC5 and *8-1trunc* parasites yield negligible signals. Scale bars, 10 μm. (C) "Zoom in" of a single *8-1* infected cell from B, showing surface distribution of luminescence signal. Scale bar, 2 μm. (D) Luminescence kinetics over parasite development, showing CLAG3 membrane insertion in *8-1* but not *8-1trunc* (red and black symbols, respectively; mean ± SEM of 3 replicate wells, representative of 3 independent trials). Enriched synchronized early ring-infected cells seeded at $t = 0$. Increased signals at 48 h in both parasites reflect parasite egress and release of intracellular reporter protein. (E) Mean ± SEM CLAG3 exposure on indicated lines at 36 h (*, $P = 0.03$; $n = 3$ trials), calculated as the luminescence signal normalized to total signal after cell lysis. (F) Mean ± SEM luminescence signals from indicated negative-control lines normalized to total signal after cell lysis, as in E. $n = 3$ independent trials for *C3-cHB* and 2 trials for *GBP-HB*. (G) Mean ± SEM luminescence signals from enriched trophozoite-infected cells without and with extracellular protease treatment (black and red bars, respectively; *, $P = 0.005$, $n = 5$).

at the host membrane (36). Both control parasites yielded negligible luminescence signals in intact cells and large signals upon lysis (Fig. 2F and Fig. S2D).

Prior studies of the CLAG3 HVR implicated exposure at the host cell surface based on this motif's susceptibility to extracellular protease (10, 26). We therefore examined whether the exposed HiBiT is also susceptible to external protease by measuring luminescence signals after a brief protease treatment of trophozoite-infected cells. While the background signal in KC5 parasites and the low-level signal from *8-1trunc* cells were not significantly affected by extracellular protease treatment ($P > 0.1$, $n = 5$ independent trials each) (Fig. 2G), the large signal produced by *8-1*-infected cells was reduced by 39% ± 3% upon treatment with extracellular protease ($P = 0.005$, $n = 5$),

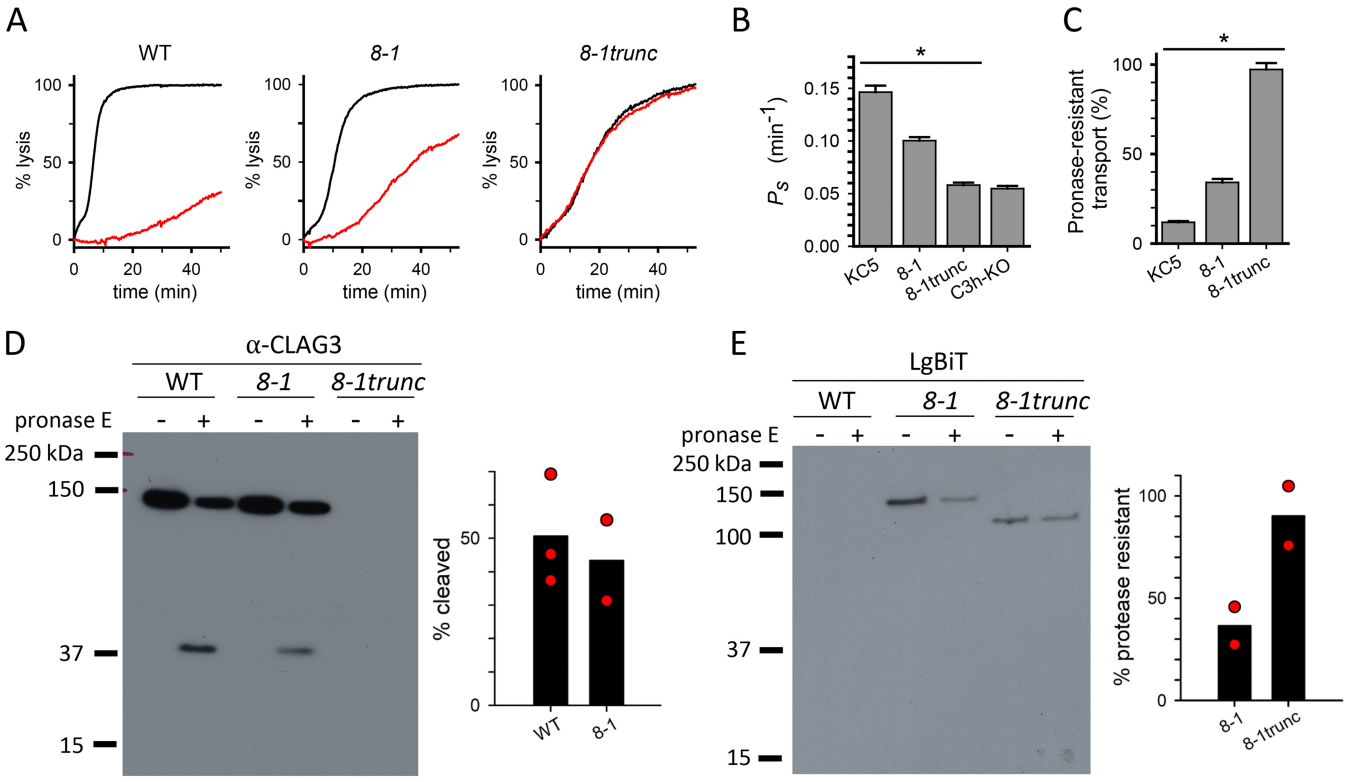

FIG 3 Modest effect of the reporter tag on CLAG3 export and on channel-mediated nutrient uptake. (A) Kinetics of osmotic lysis due to sorbitol uptake by indicated lines without or with pretreatment with pronase E (black and red traces, respectively). (B) Apparent sorbitol permeability coefficients from experiments as in A without protease treatment, calculated as 1/halftime of osmotic lysis. *, $P < 10^{-4}$; n = 4 to 21 trials each. (C) Pronase E-resistant transport activity for indicated lines, normalized to 100% for matched untreated controls. *, $P < 10^{-4}$; n = 10 to 11 trials each. (D) Anti-CLAG3 immunoblot showing a 37-kDa C-terminal cleavage product released by pronase E treatment. Bar graph shows mean fractional band intensity of the cleavage product with individual trials shown as red circles. (E) Blot probed with LgBiT showing reduction in the 150-kDa full-length CLAG3 protein upon protease treatment. Bar graph, mean band intensities after protease treatment, normalized to 100% without protease (2 trials each).

further confirming that our split NanoLuc assay faithfully reports on CLAG3 exposure at the host cell surface.

Failed export compromises channel-mediated permeability. We next examined the effects of these CLAG3 modifications on nutrient uptake at the host membrane. We tracked the uptake of sorbitol, a sugar alcohol with high PSAC permeability, and found that both the *8-1* and *8-1trunc* parasites increase host cell permeability (Fig. 3A), as expected from its requirement for intracellular pathogen survival (28, 29). Both *8-1* and *8-1trunc* parasites exhibited lower sorbitol permeabilities than the parental KC5 (Fig. 3B) ($P < 10^{-4}$, n = 20 to 21 trials each, one-way analysis of variance [ANOVA] with *post hoc* tests), but uptake was preserved to a greater extent in *8-1*. The reduced permeability in *8-1trunc* matched that of a recently reported CLAG3 knockout, *C3h-KO* ($P = 0.55$) (27), indicating that the truncated CLAG3 in this parasite does not measurably contribute to PSAC activity. Failure to traffic and insert this protein in the host membrane conservatively accounts for this phenotype (Fig. 2).

CLAG3 cleavage within the HVR by extracellular protease compromises solute transport (26). Here, we found that pronase E treatment reduced channel-mediated transport in KC5 and *8-1* but had no effect in *8-1trunc* parasites (Fig. 3A, red traces, and Fig. 3C) ($P < 10^{-4}$, n = 10 to 11 trials, one-way ANOVA with *post hoc* tests), also consistent with intracellular retention of the truncated CLAG3 protein.

Immunoblots using an antibody directed against the CLAG3 C terminus revealed single ~37-kDa cleavage products in KC5 and *8-1* (Fig. 3D), corresponding to proteolysis at the surface-exposed HVR and release of the distal fragment by pronase E. Cleaved band intensities revealed that these two parasites exported and inserted the CLAG3 protein at the host membrane with indistinguishable efficacies (Fig. 3D, bar

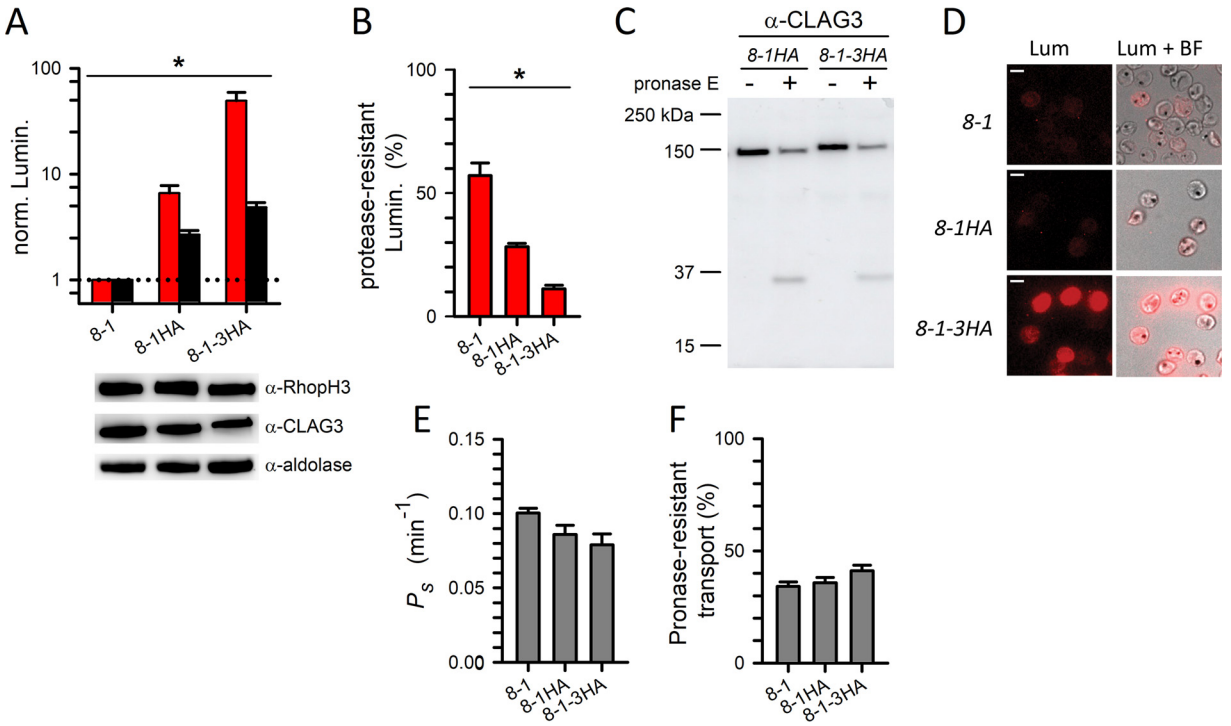

FIG 4 Addition of HA and 3×HA tags improve reporter signal and does not compromise host membrane insertion. (A) Mean ± SEM luminescence signals from indicated parasite clones using matched amounts of enriched trophozoite-infected cells. Red and black bars represent intact and lysed cells, respectively (*, $P = 10^{-4}$; one-way ANOVA; $n = 3$ independent trials). Signals are shown after normalization of corresponding *8-1* readings to 1.0 in each trial. Immunoblot shows representative loading control for matching protein contents from one of the three trials. (B) Mean ± SEM luminescence signals remaining after extracellular protease treatment of intact cells from indicated lines, normalized to 100% for no protease effect (*, $P = 0.0002$; $n = 3$ to 6 for each clone). (C) Anti-CLAG3 immunoblot showing C-terminal cleavage product released by extracellular pronase E treatment. (D) Bioluminescence microscopy showing increased signals from individual cells when 1HA and 3HA tags are added to the HiBit reporter. Scale bars, 5 μm. (E) Mean ± SEM sorbitol permeabilities for indicated parasites, determined from osmotic lysis experiments ($n = 5$ to 21 trials each). (F) Shows % of transport resistant to treatment with extracellular pronase E ($n = 4$ to 11 trials). Channel-mediated transport is affected modestly in these lines.

graph). Because *8-1trunc* parasites express a truncated CLAG3 not recognized by this antibody, we then probed these blots with LgBiT. This treatment reduced the band intensity in protein from *8-1* parasites but had a negligible effect on *8-1trunc* CLAG3 (Fig. 3E, bar graph), consistent with proteolytic degradation of an exposed HiBit tag only on *8-1* parasites.

These studies establish that CLAG3 must insert at the host membrane to contribute to PSAC activity because the truncated protein in *8-1trunc* parasites has transport activity matching that of a CLAG3-null parasite. They also reveal that proteolysis at a surface-exposed loop on CLAG3 compromises transport regardless of sequence, as this site retained its susceptibility when replaced by a HiBiT reporter.

Membrane insertion not compromised by increased extracellular loop size. To examine possible constraints on the insertion of the CLAG3 HVR at the host membrane, we generated an additional transfectant carrying a larger 3×HA epitope tag after the HiBiT cassette (see Fig. S1C in the supplemental material). Biochemical studies with *8-1HA* and this new parasite, *8-1-3HA*, revealed marked increases in luminescence signals as the extracellular loop size increased by 9 and 27 residues, respectively. Using matched numbers of trophozoite-stage parasites and normalization to the corresponding measurements from *8-1*, we found 7- and 50-fold higher luminescence signals from the *8-1HA* and *8-1-3HA* parasites (Fig. 4A, red bars). The increases in luminescence were more modest when measured after cell lysis with detergent (Fig. 4A, black bars). Greater accentuation with intact cells than after lysis is consistent with steric hindrance or constrained HiBiT presentation in a minimal extracellular loop, as proposed for CLAG3 (26). An addition of these tags also significantly increased the susceptibility of the HiBiT reporter to extracellular protease,

with the larger 3×HA tag producing a greater reduction in luminescence upon protease treatment (Fig. 4B). Membrane insertion and surface exposure were further confirmed with immunoblotting (Fig. 4C) and luminescence imaging, which revealed dramatically increased signals from intact cells (Fig. 4D). These findings suggest improved LgBiT binding and reporter complementation upon adjacent HA epitope tagging, presumably because the size and negative charge of this tag improve accessibility at the extracellular loop and within soluble RhopH complexes upon detergent release.

These larger insertions into CLAG3 produced modest reductions in channel-mediated sorbitol uptake at the host membrane (Fig. 4E). The resulting channels also retained quantitatively similar protease susceptibilities (Fig. 4F), consistent with minimally affected CLAG3 insertion and PSAC formation at the host membrane.

Larger epitopes reveal a complex regulation of CLAG3 membrane insertion. To further explore size and charge constraints on pathogen epitope presentation, we made additional transfectants containing multiple HiBiT tags with two different linker sizes (Fig. 5A). As these constructs retained upstream and distal CLAG3 sequences, each modified protein trafficked normally through schizonts and was delivered into maturing trophozoite-infected cells (see Fig. S3A and B in the supplemental material), where the increased size of the targeted protein was apparent in immunoblots (Fig. 5B). Although immunofluorescence, sorbitol permeability measurements, and protease susceptibility studies all suggested that CLAG3 failed to export and undergo host membrane insertion (see Fig. S3B in the supplemental material and Fig. 5C), bioluminescence intensity analyses using RISE nevertheless identified individual parasites that presented CLAG3 on their host cells (Fig. 5D). Notably, while most cells in each of the largest multiple HiBiT constructs produced background signals, a few cells produced very bright signals that exceeded those seen on *8-1* parasites. Imaging studies with *GBP-HB* and *C3-cHB*, negative-control parasites that export tandem HiBit constructs into the erythrocyte cytosol (Fig. S2), did not reveal similarly bright cells, indicating that infected cells do not become leaky to either NanoLuc fragment under our recording conditions. Thus, the intense signals from some cells expressing CLAG3 with multiple HiBits inserted in the variant extracellular loop cannot be explained readily by membrane leak.

The presence of markedly differing signals from individual cells is unexpected in these lines because each transfectant was cloned by limiting dilution prior to our biochemical studies. As prior studies have found that CLAG3 content and PSAC activity are both greater in erythrocytes infected with two parasites (37), we evaluated multiplicity of infection, as judged by the number of hemozoin foci in each cell. For cells infected with *8-1*, luminescence increased significantly with the number of parasites ($P < 10^{-4}$, one-way ANOVA comparison of $n = 8$ to 37 cells infected with 1, 2, or 3 parasites, which are shown as yellow, red, and blue symbols, respectively, in Fig. 5D). In contrast, the signals from cells infected with parasites carrying any of our multi-HiBit constructs were not significantly associated with parasite load ($P < 0.05$). Notably, we found that about one-half of the brightest cells (luminescence values of >1,000 arbitrary units [AU] in Fig. 5D) were infected with a single parasite, implicating additional determinants of CLAG3 presentation on the host membrane.

We tabulated the HVR sequences from 38 available CLAG3 sequences and compared their properties to those of our engineered lines. Although they are variant, the native HVR sequences tended to have a modest net negative charge (Fig. 5E, black symbols). In contrast, the constructs containing more than one HiBit epitope were increasingly basic, conferring net positive charges to the extracellular loop (Fig. 5E, red symbols). Notably, the sequence in *8-1-3HA*, whose CLAG3 successfully inserted at the host membrane to produce remarkably bright luminescence using our RISE assays, had a higher molecular weight than that of *8-2*, which failed to traffic CLAG3 protein faithfully in most cells. It appears that the domain's net positive charge in *8-2* and other multiple HiBit lines prevents trafficking and host membrane insertion. Along with structural constraints that ensure CLAG3-mediated nutrient uptake and evolutionary pressures to evade host immunity, the extracellular loop of this conserved protein family must also meet charge and size requirements for faithful trafficking and host membrane insertion.

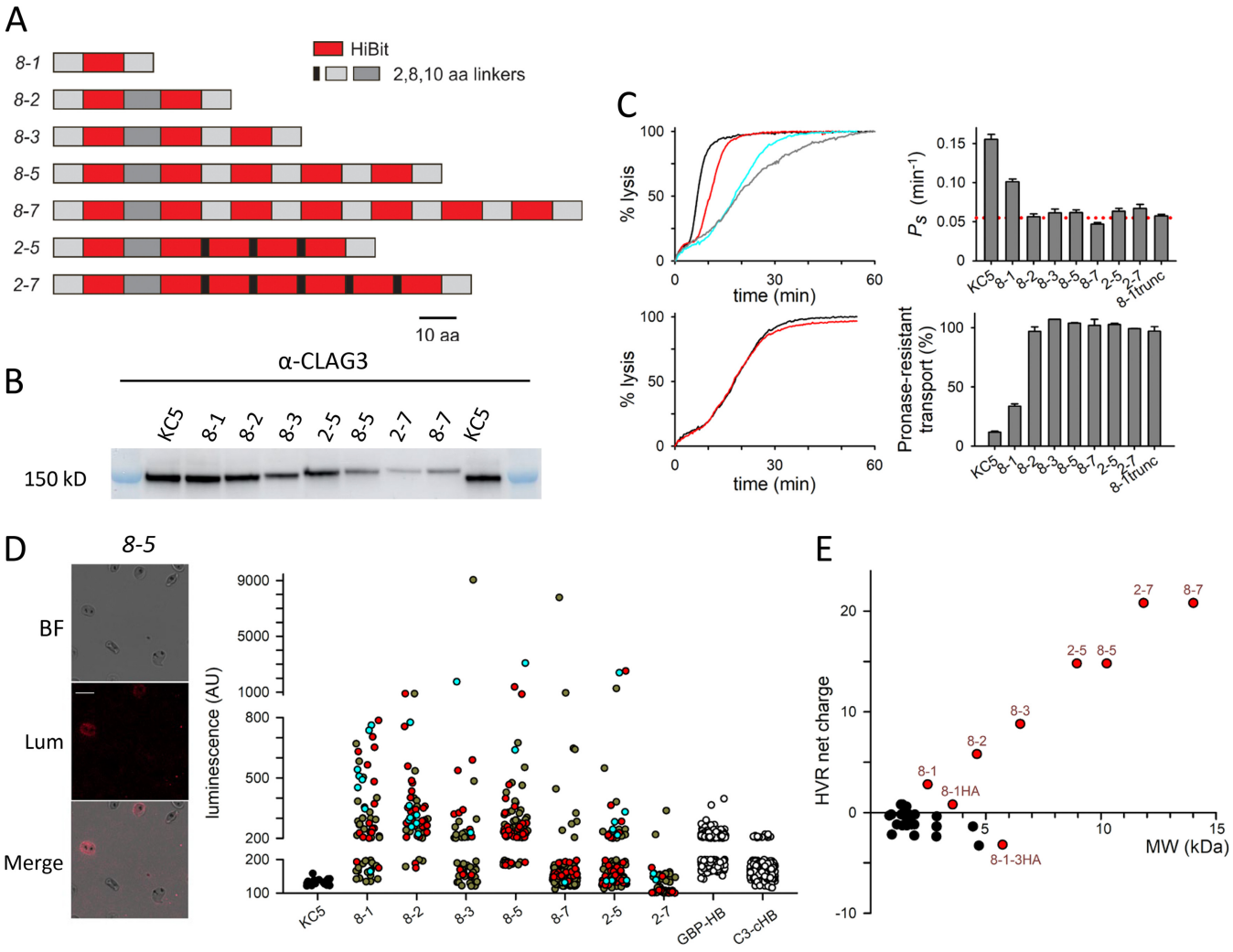

FIG 5 Large reporter inserts reveal a complex regulation of CLAG3 insertion at the host membrane. (A) To-scale schematic showing multi-HiBiT inserts and sizes of linkers between elements. The parasite names reflect the predominant linker size (in residues) followed by the number of introduced HiBiTs. (B) Anti-CLAG3 immunoblot confirming the expected increase in CLAG3 size with each construct. These match-loaded samples also suggest that constructs carrying a large number of HiBit tags may be less efficiently transferred from schizont rhoptries during erythrocyte invasion. (C) PSAC activity in transfected clones. Top left, osmotic lysis kinetics for the KC5 parent (black), *8-1* (red), *8-2* (blue), and *8-1trunc* (gray). Right, mean ± SEM of apparent sorbitol permeability coefficients for indicated lines (n = 3 to 26 trials each); red dotted line, mean for the *C3h-KO* knockout line. Note that all multi-HiBiT inserts have permeabilities indistinguishable from those of the CLAG3 knockout. Bottom left, *8-2* osmotic lysis kinetics with and without protease treatment (red and black, respectively), showing that transport is not protease sensitive in this line. Bottom right, mean ± SEM of % of transport resistant to extracellular pronase E treatment (n = 1 trial for *8-3*; 2 each for *8-5*, *2-5*, and *2–7*; 3 to 12 trials for other lines). In contrast to the CLAG3 export competent KC5 and *8-1* lines, transport linked to the multi-HiBiT inserts is resistant to extracellular pronase. (D) Microscopy images showing rare luminescent cells in the *8-5* reporter line. Jitter plot shows single-cell intensities of indicated lines (n =19 cells for KC5, 48 to 182 cells for *8-1* and the multi-HiBit lines, 243 to 300 cells for the negative-control lines *GBP-HB* and *C3-cHB*). For the following items, the symbol colors are noted: KC5 wild type, black; and negative-control transfectants, white; cells having 1, 2, or 3 multi-HiBit insert parasites, dark yellow, red, and blue, respectively. Ordinate break points were selected based on the range of intensities in the KC5 and *8-1* controls. Note that while most cells are negative in the multi-HiBiT constructs, a small number have very high signals in each reporter line; *GBP-HB* and *C3-cHB* have low signals without this variability. (E) 2D plot showing molecular weight (MW) and net charge at pH 7.4 for the CLAG3 HVR region from 38 available sequences (black circles) and the indicated engineered substitutions (red symbols).

DISCUSSION

Here, we presented a new split NanoLuc reporter that detects the insertion of pathogen virulence antigens on their host cells. This RISE assay is broadly applicable to a range of intracellular pathogens and will permit nondestructive kinetic tracking of antigen exposure at the host cell surface. Some proteins targeted to underlying membranes, such as the parasitophorous vacuolar membrane of *Plasmodia*, *Toxoplasma*, and other parasites, may also be studied using selective permeabilization of the host

membrane (38). This approach will provide quantitative insights into the presentation of targeted antigens to the host immune system and is an important step toward understanding how pathogens interact with their host cells.

The RISE assay has several advantages over traditional immunofluorescence assays for the study of antigen exposure. First, traditional confocal microscopy imaging, as used for immunofluorescence-based localization, lacks the spatial resolution required to distinguish a surface-exposed epitope from one that is associated with the cytoplasmic face of the host cell membrane; in contrast, RISE produces a signal only upon surface exposure and yielded negligible signals with tagging of the host membrane at its cytoplasmic face (Fig. 2F, C3-cHB, and Fig. S2D). Second, RISE also overcomes issues of antibody specificity and affinity, which vary for each targeted epitope and can often lead to erroneous interpretations because of cross-reactivity with other antigens. Third, RISE allows continuous tracking of antigen exposure on live cells, which is impractical with immunofluorescence-based studies. Fourth, our use of a split NanoLuc technology affords greater sensitivity than that possible with fluorescent protein reporters, whose sensitivities are limited by cellular autofluorescence. This high sensitivity and signal-to-background ratio permits both miniaturized microplate-based tracking of antigen exposure and single-cell measurements, enabling studies of cell-to-cell variation (Fig. 5). Finally, luminescence reporters avoid concerns of phototoxicity and photobleaching during acquisition. Processing of RISE samples is also much simpler than for those used in immunofluorescence as blocking, antibody addition, and wash steps are not required.

A key limitation of the RISE assay is the required insertion of a HiBit tag within a domain exposed at the host cell surface; control experiments to establish that this small tag does not alter trafficking, insertion efficacy, and biochemical properties of the target protein may be required. While macroscopic assays with this reporter can establish antigen exposure and provide quantitative kinetic information about protein export using luminometers available in most laboratories, the single-cell luminescence measurements performed here require access to a bioluminescence confocal microscope, which is currently limiting in many laboratories. As the advantages of RISE and related technologies are appreciated, these microscopes should become available more readily.

We used this new approach to propose a revised model of CLAG3 trafficking and insertion at the host erythrocyte membrane. CLAG3 produced in schizonts remains inaccessible to extracellular LgBiT upon transfer to ring-infected cells; as the intracellular parasite matures, the protein is exported and inserts in the host membrane with kinetics that parallel the gradual appearance of the associated nutrient channel activity on trophozoite-infected cells. A C-terminal truncation that does not alter the reporter or its upstream sequence compromised trafficking, abolished host membrane insertion, and reduced host cell permeability to levels seen in a recently reported CLAG3-null parasite. Using varied reporter insertions, we also uncovered complexities in this protein's export into the host cytosol and insertion at the erythrocyte membrane; our studies suggest contributions from both the size and the charge of the extracellular peptide loop.

Interestingly, a fraction of parasites carrying large multi-HiBit tags within the CLAG3 extracellular variant loop produce bright single-cell luminescence signals, implicating exposure on the host membrane. How do we reconcile this observation with our macroscopic protease susceptibility and PSAC-mediated transport measurements (Fig. 5C and S3), which do not support CLAG3 surface exposure? We excluded nonspecific leakiness of some infected cells under our imaging conditions because two negative-control parasites did not produce similarly bright signals despite exporting chimeric proteins with multiple HiBit tags into their host cytosol. One explanation for this discrepancy is that single-cell imaging studies reveal minor populations of cells capable of faithful CLAG3 presentation at the host membrane but that these rare cells fail to reach detection thresholds in macroscopic immunoblotting and transport measurements. Another possibility is that these multiple HiBit lines present CLAG3 with an altered or misfolded structure at the host membrane; such misfolded proteins may not produce functional channels or expected protease susceptibility patterns but may still be able to make high-affinity interactions with LgBit to produce

luminescence. This and other findings with our reporter lines will guide future structure-function studies of this important nutrient uptake channel.

Our luminescence imaging studies also revealed an unexpectedly large variation between cells despite the use of clonal reporter lines. We excluded cell leakiness and multiplicity of host cell infection as explanations for this variable presentation. Instead, our findings suggest epigenetic control of CLAG3 export and host membrane insertion. Such control may result either from increased *clag3* transcription to overcome defective membrane insertion of modified CLAG3 or from a posttranslational mechanism that regulates surface exposure. We propose that this may reflect altered expression of one or more parasite chaperone proteins in host cell cytosol (39) or posttranslational modifications of CLAG3 (40, 41). Our findings unveil another level of sophistication in how malaria parasites control their interactions with host plasma and evade immune attack.

We have combined RISE with a broad range of biochemical and protein chemistry approaches to examine trafficking and host membrane insertion of CLAG3, a critical determinant of parasite nutrient acquisition. Because it can be adapted readily to other intracellular pathogens and their antigens, the quantitative and sensitive RISE assay should help uncover how pathogens modify their host cells while evading immune attack.

MATERIALS AND METHODS

Parasite cultivation and transfection. The *P. falciparum* KC5 parasite clone and its engineered derivatives were cultivated in O+ human erythrocytes (Interstate Blood Bank, Inc.) at 5% hematocrit in standard RPMI 1640-based medium (KD medical) supplemented with 25 mM HEPES, 50 μg/mL hypoxanthine, 0.5% NZ microbiological bovine serum albumin (BSA; MP Biomedicals), gentamicin, and 28.6 mM $NaHCO_3$ (Gibco) at 37°C under 90% N_2, 5% CO_2, and 5% O_2 conditions.

CRISPR-Cas9 DNA transfection of parasites to produce reporter lines was performed using electroporation of pUF1-Cas9 and modified pL6 plasmids into uninfected erythrocytes as described previously (29). Plasmids were constructed using synthetic double-stranded DNA (Integrated DNA Technologies) and In-Fusion cloning (TaKaRa) into the pL6 plasmid using primers listed in Table S1 in the supplemental material. Single guide RNAs (sgRNA), selected using on-, off-, and paralog specificity scores (42), were also introduced using In-Fusion (Table S1 in the supplemental material). After erythrocyte electroporation and the addition of schizont-staged parasites, the culture was selected with 1.5 μM DSM1 and 2.5 nM WR99210. After parasite outgrowth and PCR confirmation of integration, limiting dilution cloning was performed for all transfectant lines. All experiments were performed with sequence-verified clones.

GBP-HB and *C3-cHB* were produced as negative-control episomal transfectants that export a cassette containing 5 HiBit tags followed by an HA epitope tag into the host cytosol without surface exposure. *C3-cHB* expresses a recodonized full-length CLAG3 with the cassette at its C terminus through replacement of the miniSOG tag on the pXL-M2-120w-miniSOG plasmid (24). *GBP-HB* expresses a 99-aa residue leader sequence from GBP130 (Pf3D7_1016300) followed immediately by the HiBit-HA cassette (35). A synthetic gene for this chimeric protein was cloned into pUF1-Cas9 for expression under the *pfhsp90* promoter.

Immunoblots and HiBit blots. Synchronous parasite cultures were harvested, Percoll-enriched where indicated, and used for immunoblotting experiments after hypotonic lysis (7.5 mM Na_2HPO_4, 1 mM EDTA, and 1 mM phenylmethylsulfonyl fluoride [PMSF; pH 7.5]) and solubilization in Laemmli sample buffer containing 6% SDS. When required, samples were match-loaded using turbidity measurements at 700 nm. Proteins were separated by SDS-PAGE (4 to 15% Mini-PROTEAN TGX gel; Bio-Rad) and transferred to nitrocellulose membranes. After blocking with 3% skim milk powder in 150 mM NaCl and 20 mM Tris-HCl (pH 7.4) with 0.1% Tween 20 at room temperature (RT) for 1 h, primary antibodies were applied in the same blocking buffer at a 1:1,000 to 1:3,000 dilution and incubated overnight at 4°C with gentle rocking. After three washes in 150 mM NaCl and 20 mM Tris-HCl (pH 7.4) with 0.1% Tween 20, horseradish peroxidase (HRP)-conjugated secondary antibodies were added at a 1:3,000 dilution. The blot was incubated for 1 h and washed three times. Imaging was performed after addition of Clarity Western ECL substrate (Bio-Rad) using the AI 680 imager (GE health care) or standard X-ray film exposure.

Where used, protease treatment was performed after washing and resuspending enriched trophozoite-infected cells in phosphate-buffered saline 2 (PBS-2; 150 mM NaCl, 20 mM Na_2HPO_4, 0.6 mM $CaCl_2$, and 1 mM $MgCl_2$ [pH 7.4]) at 5% hematocrit with 1 mg/mL pronase E (Sigma) for 45 to 60 min at 37°C. The treated cells and matched untreated cells were washed in PBS-2 with 1 mM PMSF at 4°C before an additional wash in this buffer with 1 mM EDTA. After hypotonic lysis, the membrane fraction was harvested by ultracentrifugation (100,000 $\times$ *g* for 1 h at 4°C) and solubilized in Laemmli sample buffer as above.

Blots probed with LgBiT used the HiBiT blotting system kit (Promega). After protein transfer, nitrocellulose membranes were washed in 150 mM NaCl and 20 mM Tris-HCl (pH 7.4) with 0.1% Tween 20. LgBiT was applied in this blotting buffer at a 1:200 dilution and incubated overnight at 4°C with gentle rocking. Furimazine was then added in blotting buffer at a 1:500 dilution before imaging as above.

Unless indicated otherwise, all immunoblots are representative of a minimum of 3 trials for each parasite shown. Band intensities were quantified using Image J software.

Coimmunoprecipitation. Schizont-stage infected cells were Percoll-sorbitol enriched and lysed with 20 volumes of 10 mM Tris (pH 7.5), 300 mM NaCl, 1% Triton X-100, and 1 mM PMSF. After a 30-min

incubation at 4°C, solubilized proteins were separated by centrifugation (14,000 × *g*, 15 min, and 4°C) and incubated with anti-HA affinity agarose beads (Sigma) with gentle mixing overnight at 4°C. After five washes, the bound protein was eluted by addition of 2.5 mg/mL HA peptide in 10 mM Tris (pH 7.5), 250 mM NaCl, and 0.1% Triton X-100 for 30 min. Eluted proteins were resuspended in Laemmli sample buffer and subjected to SDS-PAGE. Coimmunoprecipitation results are representative of at least 3 trials for each parasite shown.

Immunofluorescence assays. Indirect immunofluorescence assays were performed using air-dried thin smears after fixation with 1:1 acetone:methanol at −20°C for 2 min. Slides were then dried, blocked with 3% milk in PBS for 1 h at RT, and incubated with primary antibodies in blocking buffer (mouse anti-CLAG3, 1:100; rabbit anti-RhopH3, 1:500; mouse anti-HA, 1:100) for 1.5 h at RT under coverslips. After two washes with chilled PBS, Alexa Fluor 488 or 594-conjugated secondary antibody at a 1:500 dilution and 10 μg/mL 4′,6-diamidino-2-phenylindole (DAPI) were added in blocking buffer and incubated for 30 min at RT. After being washed and dried, slides were mounted with Prolong Diamond antifade mountant (Molecular Probes). Images were collected on a Leica SP8 microscope using a 64× oil immersion objective with serial 405-nm, 488-nm, or 594-nm excitation. Images were processed using Leica LAS X and Huygens software. For each parental line and transfectant shown, the selected images are representative of more than 100 cells observed by scanning at least 20 fields.

Enrichment of ring-infected cells. Ring-stage cultures were further synchronized by a 20-min incubation in 4% xylitol, a sugar alcohol with high PSAC permeability (43), to lyse mature infected cells. The culture was then resuspended and incubated in culture medium supplemented with 207 mM xylitol for 1 h at 37°C. This cell suspension was then layered on a discontinuous Percoll-xylitol gradient with a bottom layer of 72% Percoll and an upper layer of 40% Percoll; both solutions were prepared in RPMI 1640 medium with 208 mM xylitol, 12.4 mM HEPES, and 16.3 mg/L BSA. After centrifugation (10,000 × *g* for 30 min at 21°C), ring-stage-infected cells at 65% to 90% parasitemia were harvested and washed by dropwise addition of culture medium.

Luminescence measurements and export kinetics. Luminescence measurements were performed using Percoll-enriched infected erythrocytes in 384-well microplates using the Nano-Glo HiBiT extracellular detection system (Promega). Cells were resuspended at 0.2% hematocrit in culture medium diluted with two volumes of 100:1:2 buffer:LgBiT:furimazine, according to the manufacturer's protocol. After a 30-min RT incubation, luminescence was measured using the Centro XS3 LB 960 reader (Berthold) or Synergy Neo2 (BioTek) with a counting time of 0.5 s/well.

CLAG3 export kinetics were tracked using luminescence after seeding enriched ring-infected cells in culture medium at 0.5% hematocrit into triplicate wells at 60 μL/well. The plates were sealed with Breathe-Easy sealing membrane (RPI) and incubated at 37°C under 5% CO_2 in air. At timed intervals, 40 μL of medium from selected wells was replaced with Nano-Glo HiBiT extracellular buffer with LgBiT and furimazine substrate (Promega). Readings were taken after a 30-min room temperature incubation as described above.

Bioluminescence microscopy. Erythrocytes infected with reporter parasite clones were imaged using a LV200 inverted bioluminescence microscope with a temperature-controlled stage (Olympus). Enriched ring- or trophozoite-infected erythrocytes were resuspended in culture medium at 2.5% hematocrit before diluting 50× into Nano-Glo HiBiT extracellular buffer (Promega) with LgBiT and furimazine at 100× and 50× dilutions, respectively, for a total volume of 100 μL in a 35-mm poly-D-lysine-coated coverslip dish (MatTek). Cells were allowed to settle at 37°C for 25 min in the LV200 microscope before fields of view for imaging were selected. Bioluminescence images were collected with a 45-min exposure under a 64× oil immersion objective. Images were visualized and adjusted to 14 bit in LCmicro_2.2 software (Olympus).

Single-cell luminescence intensities were quantified using a locally developed macro that uses the corresponding brightfield image to define the cell boundary. This macro reports luminescence intensities over the cell, tabulating mean, max, and min values along with the cell two-dimensional (2D) area and is available upon request.

Osmotic lysis assays. The kinetics of PSAC-mediated sorbitol uptake and infected cell osmotic lysis were tracked continuously as described previously (27). Enriched trophozoite-stage-infected cells were washed and resuspended in 150 mM NaCl, 20 mM Na-HEPES buffer, and 0.1 mg/mL BSA (pH 7.4). Solute uptake was initiated by the addition of 280 mM sorbitol, 20 mM Na-HEPES, and 0.1 mg/mL BSA (pH 7.4). The concomitant uptake of sorbitol and water produces osmotic lysis at rates directly proportional to PSAC sorbitol permeability. Lysis kinetics were monitored continuously using transmittance of 700 nm light through the cell suspension. Osmotic lysis half-times, normalized permeability estimates, and measures of protease effect were determined from the recordings with locally developed code.

Computational and statistical analyses. CLAG3 sequences were downloaded online from http://www.plasmodb.org and aligned using Multiple Sequence Alignment (MUSCLE) to identify HVR sequences from available *P. falciparum* paralogs. The molecular weight and net charge at pH 7.4 was calculated online at http://protcalc.sourceforge.net/.

Numerical data are shown as mean ± SEM. Data were analyzed in SigmaPlot 10.0 (Systat) or Prism 8 (GraphPad). Statistical significance was determined using unpaired or paired Student's *t* test or one-way ANOVA with *post hoc* Tukey's multiple-comparison test as appropriate. Significance was accepted at a *P* value of <0.05.

SUPPLEMENTAL MATERIAL

Supplemental material is available online only.

FIG S1, TIF file, 2.2 MB.

FIG S2, TIF file, 1.7 MB.

FIG S3, PDF file, 0.6 MB.

ACKNOWLEDGMENTS

We thank Gagan Saggu for help with immunofluorescence assays and David Jacobus for WR99210. DSM1 (MRA-1161) was obtained through MR4 as part of the BEI Resources Repository, NIAID, NIH.

We declare that no competing interests exist.

This study was supported by the Intramural Research Program of National Institutes of Health, National Institute of Allergy and Infectious Diseases. The funders had no role in study design, data collection and analysis, decision to publish, or preparation of the manuscript.

REFERENCES

1. Thakur A, Mikkelsen H, Jungersen G. 2019. Intracellular pathogens: host immunity and microbial persistence strategies. J Immunol Res 2019:1356540. https://doi.org/10.1155/2019/1356540.
2. Cornejo E, Schlaermann P, Mukherjee S. 2017. How to rewire the host cell: a home improvement guide for intracellular bacteria. J Cell Biol 216:3931–3948. https://doi.org/10.1083/jcb.201701095.
3. Marti M, Baum J, Rug M, Tilley L, Cowman AF. 2005. Signal-mediated export of proteins from the malaria parasite to the host erythrocyte. J Cell Biol 171:587–592. https://doi.org/10.1083/jcb.200508051.
4. Laliberte J, Carruthers VB. 2008. Host cell manipulation by the human pathogen *Toxoplasma gondii*. Cell Mol Life Sci 65:1900–1915. https://doi.org/10.1007/s00018-008-7556-x.
5. Lee WC, Russell B, Renia L. 2019. Sticking for a cause: the falciparum malaria parasites cytoadherence paradigm. Front Immunol 10:1444. https://doi.org/10.3389/fimmu.2019.01444.
6. Yam XY, Preiser PR. 2017. Host immune evasion strategies of malaria blood stage parasite. Mol Biosyst 13:2498–2508. https://doi.org/10.1039/c7mb00502d.
7. Desai SA. 2014. Why do malaria parasites increase host erythrocyte permeability? Trends Parasitol 30:151–159. https://doi.org/10.1016/j.pt.2014.01.003.
8. Mayhew TM, Lucocq JM. 2008. Developments in cell biology for quantitative immunoelectron microscopy based on thin sections: a review. Histochem Cell Biol 130:299–313. https://doi.org/10.1007/s00418-008-0451-6.
9. Nilsson Bark SK, Ahmad R, Dantzler K, Lukens AK, De Niz M, Szucs MJ, Jin X, Cotton J, Hoffmann D, Bric-Furlong E, Oomen R, Parrington M, Milner D, Neafsey DE, Carr SA, Wirth DF, Marti M. 2018. Quantitative proteomic profiling reveals novel *Plasmodium falciparum* surface antigens and possible vaccine candidates. Mol Cell Proteomics 17:43–60. https://doi.org/10.1074/mcp.RA117.000076.
10. Nguitragool W, Bokhari AA, Pillai AD, Rayavara K, Sharma P, Turpin B, Aravind L, Desai SA. 2011. Malaria parasite *clag3* genes determine channel-mediated nutrient uptake by infected red blood cells. Cell 145:665–677. https://doi.org/10.1016/j.cell.2011.05.002.
11. Jouin H, Goguet de la Salmoniere YO, Behr C, Huyin Qan Dat M, Michel JC, Sarthou JL, Pereira da Silva L, Dubois P. 1995. Flow cytometry detection of surface antigens on fresh, unfixed red blood cells infected by *Plasmodium falciparum*. J Immunol Methods 179:1–12. https://doi.org/10.1016/0022-1759(94)00265-x.
12. Florens L, Liu X, Wang Y, Yang S, Schwartz O, Peglar M, Carucci DJ, Yates JR, III, Wu Y. 2004. Proteomics approach reveals novel proteins on the surface of malaria-infected erythrocytes. Mol Biochem Parasitol 135:1–11. https://doi.org/10.1016/j.molbiopara.2003.12.007.
13. Cohn JV, Alkhalil A, Wagner MA, Rajapandi T, Desai SA. 2003. Extracellular lysines on the plasmodial surface anion channel involved in Na^+ exclusion. Mol Biochem Parasitol 132:27–34. https://doi.org/10.1016/j.molbiopara.2003.08.001.
14. Taraschi TF, Trelka D, Martinez S, Schneider T, O'Donnell ME. 2001. Vesicle-mediated trafficking of parasite proteins to the host cell cytosol and erythrocyte surface membrane in *Plasmodium falciparum* infected erythrocytes. Int J Parasitol 31:1381–1391. https://doi.org/10.1016/S0020-7519(01)00256-9.
15. Papakrivos J, Newbold CI, Lingelbach K. 2005. A potential novel mechanism for the insertion of a membrane protein revealed by a biochemical analysis of the *Plasmodium falciparum* cytoadherence molecule PfEMP-1. Mol Microbiol 55:1272–1284. https://doi.org/10.1111/j.1365-2958.2004.04468.x.
16. Wehrman TS, Casipit CL, Gewertz NM, Blau HM. 2005. Enzymatic detection of protein translocation. Nat Methods 2:521–527. https://doi.org/10.1038/nmeth771.
17. Joffre OP, Segura E, Savina A, Amigorena S. 2012. Cross-presentation by dendritic cells. Nat Rev Immunol 12:557–569. https://doi.org/10.1038/nri3254.
18. Azevedo MF, Nie CQ, Elsworth B, Charnaud SC, Sanders PR, Crabb BS, Gilson PR. 2014. *Plasmodium falciparum* transfected with ultra bright NanoLuc luciferase offers high sensitivity detection for the screening of growth and cellular trafficking inhibitors. PLoS One 9:e112571. https://doi.org/10.1371/journal.pone.0112571.
19. Dixon AS, Schwinn MK, Hall MP, Zimmerman K, Otto P, Lubben TH, Butler BL, Binkowski BF, Machleidt T, Kirkland TA, Wood MG, Eggers CT, Encell LP, Wood KV. 2016. NanoLuc complementation reporter optimized for accurate measurement of protein interactions in cells. ACS Chem Biol 11:400–408. https://doi.org/10.1021/acschembio.5b00753.
20. Knuepfer E, Rug M, Klonis N, Tilley L, Cowman AF. 2005. Trafficking of the major virulence factor to the surface of transfected *P falciparum*-infected erythrocytes. Blood 105:4078–4087. https://doi.org/10.1182/blood-2004-12-4666.
21. Llora-Batlle O, Tinto-Font E, Cortes A. 2019. Transcriptional variation in malaria parasites: why and how. Brief Funct Genomics 18:329–341. https://doi.org/10.1093/bfgp/elz009.
22. Cortes A, Carret C, Kaneko O, Yim Lim BY, Ivens A, Holder AA. 2007. Epigenetic silencing of *Plasmodium falciparum* genes linked to erythrocyte invasion. PLoS Pathog 3:e107. https://doi.org/10.1371/journal.ppat.0030107.
23. Iriko H, Kaneko O, Otsuki H, Tsuboi T, Su XZ, Tanabe K, Torii M. 2008. Diversity and evolution of the *rhoph1/clag* multigene family of *Plasmodium falciparum*. Mol Biochem Parasitol 158:11–21. https://doi.org/10.1016/j.molbiopara.2007.11.004.
24. Gupta A, Balabaskaran-Nina P, Nguitragool W, Saggu GS, Schureck MA, Desai SA. 2018. CLAG3 self-associates in malaria parasites and quantitatively determines nutrient uptake channels at the host membrane. mBio 9:e02293-17. https://doi.org/10.1128/mBio.02293-17.
25. Gupta A, Thiruvengadam G, Desai SA. 2015. The conserved *clag* multigene family of malaria parasites: essential roles in host-pathogen interaction. Drug Resist Updat 18:47–54. https://doi.org/10.1016/j.drup.2014.10.004.
26. Nguitragool W, Rayavara K, Desai SA. 2014. Proteolysis at a specific extracellular residue implicates integral membrane CLAG3 in malaria parasite nutrient channels. PLoS One 9:e93759. https://doi.org/10.1371/journal.pone.0093759.
27. Gupta A, Bokhari AAB, Pillai AD, Crater AK, Gezelle J, Saggu G, Nasamu AS, Ganesan SM, Niles JC, Desai SA. 2020. Complex nutrient channel phenotypes despite Mendelian inheritance in a *Plasmodium falciparum* genetic cross. PLoS Pathog 16:e1008363. https://doi.org/10.1371/journal.ppat.1008363.
28. Pillai AD, Nguitragool W, Lyko B, Dolinta K, Butler MM, Nguyen ST, Peet NP, Bowlin TL, Desai SA. 2012. Solute restriction reveals an essential role for *clag3*-associated channels in malaria parasite nutrient acquisition. Mol Pharmacol 82:1104–1114. https://doi.org/10.1124/mol.112.081224.
29. Ito D, Schureck MA, Desai SA. 2017. An essential dual-function complex mediates erythrocyte invasion and channel-mediated nutrient uptake in malaria parasites. Elife 6:e23485. https://doi.org/10.7554/eLife.23485.
30. Ben Chaabene R, Lentini G, Soldati-Favre D. 2021. Biogenesis and discharge of the rhoptries: key organelles for entry and hijack of host cells by the Apicomplexa. Mol Microbiol 115:453–465. https://doi.org/10.1111/mmi.14674.
31. Schureck MA, Darling JE, Merk A, Shao J, Daggupati G, Srinivasan P, Olinares PDB, Rout MP, Chait BT, Wollenberg K, Subramaniam S, Desai SA. 2021. Malaria parasites use a soluble RhopH complex for erythrocyte invasion and an integral form for nutrient uptake. Elife 10:e65282. https://doi.org/10.7554/eLife.65282.
32. Ling IT, Florens L, Dluzewski AR, Kaneko O, Grainger M, Yim Lim BY, Tsuboi T, Hopkins JM, Johnson JR, Torii M, Bannister LH, Yates JR, III, Holder AA, Mattei D. 2004. The *Plasmodium falciparum clag9* gene encodes a rhoptry protein

that is transferred to the host erythrocyte upon invasion. Mol Microbiol 52:107–118. https://doi.org/10.1111/j.1365-2958.2003.03969.x.
33. Ho CM, Jih J, Lai M, Li X, Goldberg DE, Beck JR, Zhou ZH. 2021. Native structure of the RhopH complex, a key determinant of malaria parasite nutrient acquisition. Proc Natl Acad Sci U S A 118:e2100514118. https://doi.org/10.1073/pnas.2100514118.
34. Kutner S, Baruch D, Ginsburg H, Cabantchik ZI. 1982. Alterations in membrane permeability of malaria-infected human erythrocytes are related to the growth stage of the parasite. Biochim Biophys Acta 687:113–117. https://doi.org/10.1016/0005-2736(82)90178-X.
35. Boddey JA, Moritz RL, Simpson RJ, Cowman AF. 2009. Role of the Plasmodium export element in trafficking parasite proteins to the infected erythrocyte. Traffic 10:285–299. https://doi.org/10.1111/j.1600-0854.2008.00864.x.
36. Sharma P, Rayavara K, Ito D, Basore K, Desai SA. 2015. A CLAG3 mutation in an amphipathic transmembrane domain alters malaria parasite nutrient channels and confers leupeptin resistance. Infect Immun 83:2566–2574. https://doi.org/10.1128/IAI.02966-14.
37. Ahmad M, Manzella-Lapeira J, Saggu G, Ito D, Brzostowski JA, Desai SA. 2020. Live-cell FRET reveals that malaria nutrient channel proteins CLAG3 and RhopH2 remain associated throughout their tortuous trafficking. mBio 11:e01354-20. https://doi.org/10.1128/mBio.01354-20.
38. Jackson KE, Spielmann T, Hanssen E, Adisa A, Separovic F, Dixon MW, Trenholme KR, Hawthorne PL, Gardiner DL, Gilberger T, Tilley L. 2007. Selective permeabilization of the host cell membrane of *Plasmodium falciparum*-infected red blood cells with streptolysin O and equinatoxin II. Biochem J 403:167–175. https://doi.org/10.1042/BJ20061725.
39. Zhang Q, Ma C, Oberli A, Zinz A, Engels S, Przyborski JM. 2017. Proteomic analysis of exported chaperone/co-chaperone complexes of *P falciparum* reveals an array of complex protein-protein interactions. Sci Rep 7:42188. https://doi.org/10.1038/srep42188.
40. Cobbold SA, Santos JM, Ochoa A, Perlman DH, Llinas M. 2016. Proteome-wide analysis reveals widespread lysine acetylation of major protein complexes in the malaria parasite. Sci Rep 6:19722. https://doi.org/10.1038/srep19722.
41. Pease BN, Huttlin EL, Jedrychowski MP, Talevich E, Harmon J, Dillman T, Kannan N, Doerig C, Chakrabarti R, Gygi SP, Chakrabarti D. 2013. Global analysis of protein expression and phosphorylation of three stages of *Plasmodium falciparum* intraerythrocytic development. J Proteome Res 12:4028–4045. https://doi.org/10.1021/pr400394g.
42. Ribeiro JM, Garriga M, Potchen N, Crater AK, Gupta A, Ito D, Desai SA. 2018. Guide RNA selection for CRISPR-Cas9 transfections in *Plasmodium falciparum*. Int J Parasitol 48:825–832. https://doi.org/10.1016/j.ijpara.2018.03.009.
43. Bokhari AA, Solomon T, Desai SA. 2008. Two distinct mechanisms of transport through the plasmodial surface anion channel. J Membrane Biol 226:27–34. https://doi.org/10.1007/s00232-008-9136-2.